Progress In Electromagnetics Research, Vol. 137, 129–147, 2013

A NOVEL, HIGH-SPEED IMAGE TRANSMITTER FOR WIRELESS CAPSULE ENDOSCOPY

Md. R. Basar[1, *], Fareq Malek[2], Mohd I. M. Saleh[3], Mohd S. Idris[3], Khairudi M. Juni[3], Azuwa Ali[2], Nur A. Mohd Affendi[2], and Nuriziani Hussin[2]

[1]School of Computer and Communication Engineering, Universiti Malaysia Perlis (UniMAP), Kuala Perlis, Perlis 02000, Malaysia

[2]School of Electrical Systems Engineering, Universiti Malaysia Perlis (UniMAP), Pauh Putra, Arau, Perlis 02600, Malaysia

[3]Electrical Engineering Department, Politeknik Tuanku Syed Sirajuddin (PTSS), Pauh Putra, Perlis 02600, Malaysia

Abstract—Wireless capsule endoscopy (WCE) was developed as a painless diagnostic tool for endoscopic examination of the gastrointestinal (GI) tract, but, to date, the low operating power of the capsule and the high data rate of the RF telemetry system are still key concerns. Innovative, novel solutions must be developed to address these concerns before WCE can be used extensively in clinical applications. In this paper, we propose a novel RF transmitter for WCE applications that only requires 1.5 V to transmit the required data as opposed to using a DC power supply. Our proposed, direct-conversion transmitter system consists of a current reuse oscillator, an envelope filter, and an L-section matching network. The oscillator is powered by the transmitting data which keep the oscillator in turned on and off for the transmitting 1 and 0 bit respectively and results in the on-off keying (OOK) of the modulated signal at the output of the oscillator. The rate of data transmission at the modulated signal is limited by the transient period of the oscillator start-up. When the start-up time of the oscillator is optimized, an OOK modulation rate of 100 Mb/s can be attained. In order to eliminate the oscillator decay noise, we used an envelope filter connected in series with the oscillator to filter out the decay part of the oscillation. Finally, the output impedance of the envelope filter is matched to the 50-Ω antenna with an L-section, low-pass, matching network to ensure maximum

Received 11 January 2013, Accepted 6 February 2013, Scheduled 14 February 2013

* Corresponding author: Md. Rubel Basar (rubel24434@yahoo.com).

power transmission. The entire transmitter system was simulated in a 0.18- μm Complementary metal-oxide-semiconductor (CMOS) process.

1. INTRODUCTION

Endoscopy is a system that makes it possible to conduct visual examinations inside the body for medical reasons. The development of ingestible wireless capsule endoscopy (WCE) [1] is viewed as a revolutionary advancement in gastrointestinal (GI) tract endoscopy. This emerging technique overcame the previous complexities associated with inspecting the entire small intestine, which is the most complex part of the GI tract and is unreachable by conventional probe endoscopy. However, the most important parameters of the capsule are its power consumption, image resolution, and the rate at which it can transmit images. Presently, reducing the capsule's power consumption and having it achieve a higher image-transmission rate are the key issues that stand in the way of more extensive applications of WCE in clinical settings. Thus, much of the ongoing research is focused on the development of telemetry systems that require less power and provide higher rates of data transmission of high resolution images [2, 3].

The first clinical capsule, developed by Given Imaging, uses a transmitter chip produced by Zarlink Semiconductor, Inc. (Canada) that has a transmission capacity of 2.7 Mb/s, which can transmit 320×320 pixel images at a rate of 2 frames per second, and a power consumption of 5.2 mW [3]. Subsequently, many RF telemetry systems for WCE have been developed that reduced power consumption and improved the data transmission rate. Currently, the super-heterodyne architecture is the preferred choice for the RF transceiver due to its superior sensitivity, frequency stability, and selectivity. For WCE applications, a super-heterodyne transmitter and receiver have been implemented on a single chip in [4, 5], and the transmitter consists of an on-chip voltage-controlled oscillator (VCO), an amplitude-shift keying (ASK) modulator, an up-converter, a 20-MHz intermediate-frequency (IF) phase-locked loop (PLL), and an radio frequency (RF) output buffer with an off-chip, crystal oscillator. The transmitter of the super-heterodyne architecture is optimized to an optimum power consumption of 14 mW because it consists of many building blocks, which results in increased power consumption. In order to accomplish the low power and high data rate requirements, the impulse radio ultra-wide band (IR-UWB) [6–9] technology is a candidate technology that potentially could meet the requirements of low power usage and high data transmission rate. A UWB-OOK system was developed in [7], and it provided data transmission rates up to 10 Mbps, and it was capable

of transmitting images with resolutions of 640×480 pixels at the rate of 2.5 frames/s. The use of the UWB technique in WCE is problematic because its high frequency carrier is attenuated significantly by the biological tissue that makes up the walls of the small intestine [10, 11]. The direct conversion transmitter architecture is the most popular in biomedical applications because of the simplicity of its circuitry and its low power consumption [7, 12–14]. Diao et al. proposed a direct conversion ASK transmitter that could attain a data transmission rate of 15 Mbps with a power consumption 7.2 mW. Kim et al. made a significant contribution to this field by developing a high-speed, high-efficiency capsule endoscopy system [14]. The direct conversion RF transmitter of their system can transmit image data at the rate of 20 Mb/s while consuming DC power of less than 3 mW; the 20-Mbps channel can transmit images with resolutions of 640×480 at a rate of eight frames per second without compression. Clearly, the proposed telemetry systems for WCE are incapable of transmitting images at the rate of 30 frames per second.

Thus, in pursuit of the goal of providing a novel telemetry system for use in WCE that allows the rapid transmission of high-quality images but has a low power requirement, we propose a novel OOK RF transmitter that has a high data transmission rate. The important advantage of our proposed transmitter is that it can operate with power at the 1.5 V DC level and transmit data at the rate of 100 Mb/s.

2. DESIGN CONSIDERATION

2.1. Frequency Approach

The optimum selection of the frequency of the system improves its performance [15–17]. This selection is most important for WCE applications, because the frequency-dependent, dielectric properties of the human body are highly hostile to the propagation of RF signals [18, 19]. The attenuation of the power of the signal by the human body varies remarkably with the frequency [20]. Many different RF telemetry systems have been proposed in the literature for WCE with the arbitrary selection of frequencies without appropriate attention to the importance of the frequency, including a 2.4-GHz, high-data-rate transceiver [4]; a low-power, 3–5-GHz, ultra-wideband transceiver [7]; a 15-Mbps, 900-MHz ASK transmitter [13]; a 0.5-GHz, high-speed, high-efficiency system [14]; and a 1.4-GHz conformal, ingestible, capsule antenna [21]. In this regard, the IEEE 802.15.6 standard specifies a frequency band of 402–405 MHz for a wireless body area network (WBAN) [22]. But its 3-MHz channel is not sufficient for a high rate of data transmission in WCE applications. In the analysis of

the characteristics of radiation in the range of 150 MHz to 1.2 GHz from inside the human body done by [23], it was suggested that frequencies between 450 MHz and 900 MHz provided maximum radiation from the ingested RF source. Using the human body model [24–29] in our previous work [10], we conducted an extensive investigation of the variation of path loss in the human body in terms of system frequency and variation of the location of the capsule. A summary of the results of our investigation are shown in Figure 1. Clearly, the relationship between path loss and frequency differs from region to region in the GI tract, but the average graph shows that the path loss was less significant beyond 500 MHz. Thus, we considered bandwidths between 400 and 500 MHz, i.e., about 450 MHz, to be the most suitable selection for a telemetry system to be used in WCE.

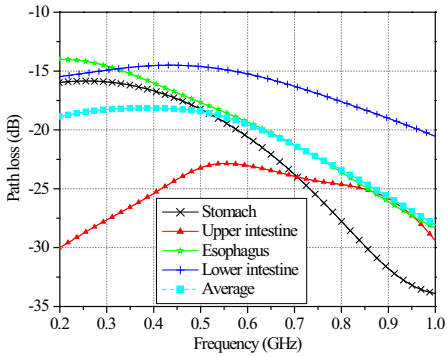

Figure 1. Variation of path loss in the human body.

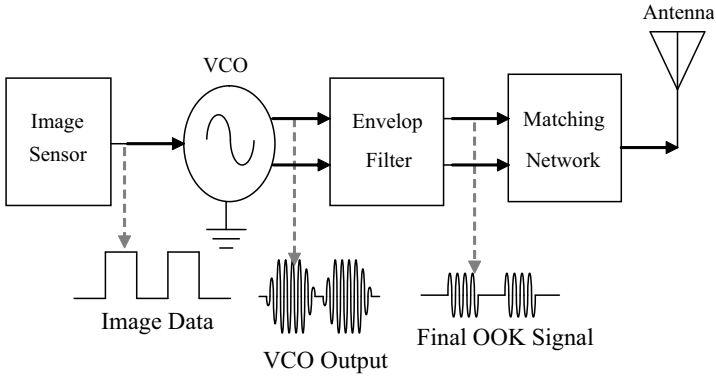

Figure 2. Architecture of proposed, novel, high speed transmitter.

2.2. System Approaches

The main challenges in designing an RF circuit for biomedical applications are minimizing the size and reducing the power requirement. There are several methods that can produce a low-power, RF circuit. In general, the entire power budget of the systems is dominated by the selection of the system architecture, the modulation scheme, and the optimization of the designs of the basic building blocks, such as VCO and matching networks. However, by combining several of these low-power designs, it is possible to achieve an ultra-low power design. In this regard, several transmitter architectures are used commonly in RF systems, such as super-heterodyne, low IF, direct conversion, and zero-IF architectures. All of these architectures have advantages and disadvantages, but, considering the power required and the space required for circuit elements, direct conversion is a more attractive choice than super-heterodyne for use in an implantable medical RF device [30]. Considering the simplicity of the transmitter and receiver system, power consumption, receiver sensitivity, and the required bandwidth, on-off keying (OOK) is the most efficient modulation scheme. With this consideration, our proposed transmitter architecture is shown in Figure 2. The different low-power approaches that were incorporated in this architecture are shown in Table 1. The entire transmitter system contains three main basic building blocks, i.e., the oscillator, the envelop filter, and the output matching network. In our proposed system, the OOK modulation scheme was integrated into the simplified, current-reuse oscillator. The OOK transmitter consumed only 50% of the power consumed by a

Table 1. Low-power techniques used in the architecture of the proposed transmitter.

Options	Used in this work	Advantage
Transmitter architecture	Direct conversion	Low power and circuit simplicity
VCO topology	Current reuse VCO	Operates at half the power of a conventional LC VCO
Modulation	OOK	No power consumption for 0 bit transmission
Technology	CMOS, 0.18 µm	Easy to fabricate
System frequency	450 MHz	Optimum path loss in the human body

typical, frequency-shift keying (FSK) transmitter because power is required only for transmitting 1 bit; during 0-bit transmission, the transmitter does not consume any power. In addition, the simplified, current-reuse VCO scheme consumes power from a DC source only for one-half of its oscillation cycle; for the next half-cycle, it reuses its tank-discharging current. Used together, these two techniques (integrated OOK and current reuse VCO) reduce the power demand of our proposed transmitter to only 25% of the power required by a conventional RF transmitter. The power amplifier uses the most power of any component in the transmitter, so it was excluded from the architecture of the transmitter, while the peak-to-peak output voltage switching of the oscillator was optimized for sufficient output power.

3. CIRCUIT DESIGN

3.1. Oscillator Circuit

The oscillator core is shown in the left, dashed block of the proposed transmitter circuit in Figure 3, where the stacking switches PMOS (M_1) and NMOS (M_2), connected in series with the LC tank, construct the simplified, current-reuse topology of the oscillator. The operation of the simplified, current-reuse, voltage-control oscillator (VCO) was discussed in detail in our previous work [31]. Although the values of L_1 and C_1 in the circuit of the LC tank conventionally can be determined by using Equation (1), the values of L_1 and C_1 have a great impact on swings in the oscillator's output voltage, start-up transient time, and phase noise PN.

$$f = \frac{1}{2\pi}\sqrt{\frac{1}{LC}}, \tag{1}$$

where, f is the frequency of oscillation. In order to obtain the optimum swings in the voltage, PN, and fast start-up time, it is recommended that the maximum possible value for L be chosen [32]. The PN of oscillator can be estimated using following equation.

$$\begin{aligned} R_{eff} &= \frac{2\pi f L}{Q} \\ PN &= \frac{2KTR_{eff}[1+A]\omega_o^2}{V^2(\Delta\omega)^2}, \end{aligned} \tag{2}$$

where, A is the start-up safety factor, ω_o is frequency of oscillation, $\Delta\omega$ is the offset frequency, and V is the peak output amplitude. The losses across the tank circuit can be determine either by using the relation $R_L = Q\omega_o L$ (where Q is the quality factor of the tank and is almost equal to the quality factor of L) or by AC simulation of the

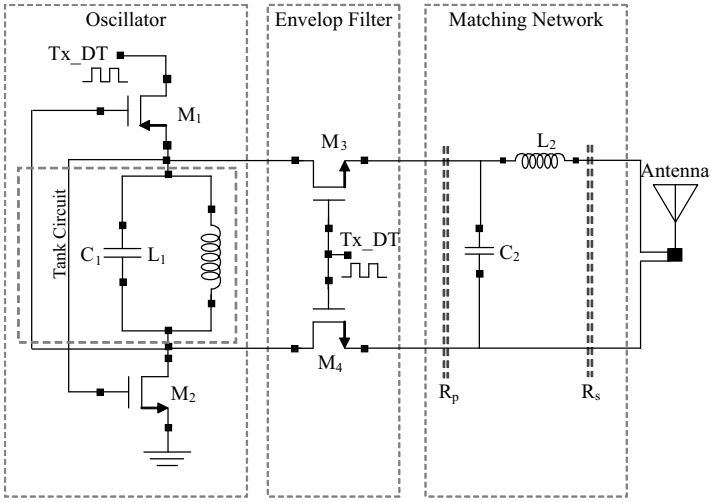

Figure 3. Proposed transmitter circuit.

tank circuit. To initiate oscillation, the transconductance, G_m, of the active device (stacking switch M_1 and M_2) must be greater than $1/R_L$. Therefore, the gate width (W) and length (L) of the active devices can be adjusted by using Equation (3).

$$G_{m(M_1/M_2)} = \sqrt{2\mu_{(p/n)}C_{ox}\frac{W}{L}I_D}, \tag{3}$$

where, $\mu_{p/n}$ is the carrier's mobility of P-type/N-type material and C_{ox} is the gate capacitance per unit area.

Note that the trasnconductances of M_1 and M_2 are the same, which results in a better PN performance of the oscillator [32, 33] and requires the following design conditions:

$$\sqrt{2\mu_p C_{ox}\frac{W_{M_1}}{L_{M_1}}I_{DS}} = \sqrt{2\mu_n C_{ox}\frac{W_{M_2}}{L_{M_2}}I_{DS}}$$

$$\mu_p\frac{W_{M_1}}{L_{M_1}} = \mu_n\frac{W_{M_2}}{L_{M_2}}$$

These two equations refer to the ratio of the lengths of NMOS and PMOS, which is:

$$\frac{L_{M_2}}{L_{M_1}} = \sqrt{\frac{\mu_n}{\mu_p}}$$

The length of the MOS transistor is set to the minimum allowed by the technology, which refers to the ratio of the width of PMOS to the

width of NMOS, i.e.,

$$\frac{W_{M_1}}{W_{M_2}} = \sqrt{\frac{\mu_n}{\mu_P}} \tag{4}$$

Due to the fact that the P-type material has lower carrier's mobility (μ_p) than the N-type material (μ_n), the gate width of M_1 is greater than that of M_2, resulting in better PN performance.

3.2. Optimization of Start-up Time

The duration of the oscillator's start-up transient generally is not considered to be an important parameter because the oscillator operates continuously in most RF systems [34]. The duration of the start-up transient is of great interest to designers of impulse radio ultra-wideband (IR-UWB) transmitter systems [35, 36]. In order to analyze the delay in the oscillator's start up, the oscillator's response to a pulse input can be described as shown in Figure 4, in which the different phases, the start-up period, the steady-state period, and the decay period are represented by t_{s-u},t_{s-s}, and t_d. In our proposed OOK transmitter, the oscillator is turned on and off by 1 bit and 0 bit, respectively. In order to transmit the data bits successfully, the oscillator must satisfy the condition $t_{s-u} \ll PW$. As the width of the pulse becomes shorter as the rate of data transmission increases, it becomes more and more difficult to reduce the start-up time. However, the start-up time can be reduced by a complex circuit that provides additional biasing current, but that requires additional power [37]. However, the matching gate capacitances of NMOS and PMOS of the active network and tank circuit optimization, neither of which requires additional circuits, can reduce the start-up time [37, 38]. The matching

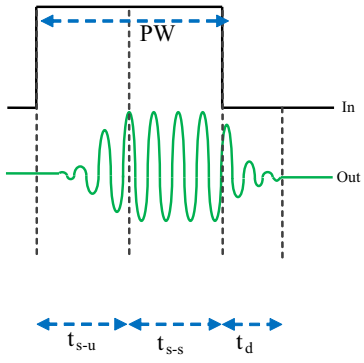

Figure 4. Response of the oscillator to a pulse input.

gate capacitances of both M_1 and M_2 require that:

$$W_{M_1} L_{M_1} = W_{M_2} L_{M_2} \tag{5}$$

3.3. Envelop Filter

At high-speed transmission, the decay time of the oscillator is greater than the duration of 0 bit. Thus, remarkable power is added to 0 bit as a result of the decay of the oscillation. This unexpected power causes noise in the envelope signal, which can result in erroneous detection. In order to overcome this problem, an envelope filter (middle dashed box of Figure 3) designed with two series NMOS (M_3 and M_4) was used to eliminate the decay signal of the oscillator.

3.4. Matching Network

In order to minimize the loss due to reflection and to maximize transmission, matching networks were used between the two system blocks. These networks eliminated unwanted resistance for a range of frequencies. Due to the lower efficiency of the T and Π matching networks [39], the L-section matching network is commonly used. The efficiency of the L-section matching network depends on the impedance transformation ratio, the quality factor of the lumped elements, and the optimum number of L-section stages. The impedance transformation ratio and the quality factor of the lumped elements are fixed by the system blocks to be matched and the used technology respectively. In this case the matching efficiency can be improved by using optimum number of L-section stages. The optimum number of stages can be obtained by using following the following formula [40]:

$$\begin{aligned} n_{opt} &\to [\ln Q], \\ \text{where } \; Q &= \sqrt{\frac{R_p}{R_s} - 1} \end{aligned} \tag{6}$$

According to (6), the single L-section, low-pass, high-to-low transformation, impedance matching network that we designed is shown in the last dashed box of Figure 3, in which the values of the lumped elements C_2 and L_2 are determined by Equations (7) and (8) [41]:

$$C_2 = \frac{Q}{2\pi f R_p} \tag{7}$$

$$L_2 = \frac{Q R_s}{2\pi f} \tag{8}$$

4. RESULTS AND DISCUSSION

The entire transmitter system was simulated in advanced design system (ADS) using Taiwan Semiconductor Manufacturing Company (TSMC) 0.18-µm CMOS process. Throughout the design, the gate length of the MOS transistor that we used was 0.18 µm, which was the minimum length supported by the technology. In order to oscillate at a frequency of 450 MHz, L_1 and C_1 initially were set to 17 nH and 7 pF, respectively, by Equation (1). According to the Equation (4) the length of active devices (M_1 and M_2) W_{M_1} and W_{M_2} were set to 100 µm, and 70 µm respectively. With this design, the oscillator was simulated with 1.5 V DC and achieved the best PN, i.e., −137 dBc at 1 MHz offset (Figure 5(a)). Figure 5(b) shows the frequency spectrum of the oscillating signal, which has a power ratio of 10.887 dBm at the center frequency.

Finally, the 1.5 V DC source was replaced by pulse data with a V-low of 0 V and a V-high of 1.5 V. The oscillator was operated at a frequency of 450 MHz for V-high and was kept off for V-low, which produced an OOK modulated signal. Figure 6 shows the OOK modulated signal at three different data transmission rates, i.e., 20 Mb/s, 40 Mb/s, and 100 Mb/s. Clearly, the figure shows that, as the data transmission rate increased, the initial bit missing increased beyond the rate 20 Mp/s because of the slow start-up time. At the higher data transmission rate, the duration of V-high was shorter than t_{s-u}, which turned the oscillator off before it was fully operational. Therefore, an oscillator that starts up rapidly can achieve a high data transmission rate OOK signal without bit missing.

A complex, tail current-biasing circuit can reduce the start-

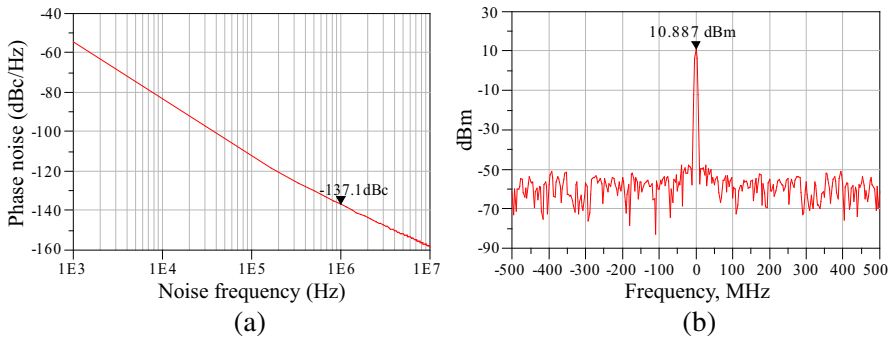

Figure 5. (a) Oscillator phase noise. (b) Carrier spectrum (at a frequency of 450 MHz).

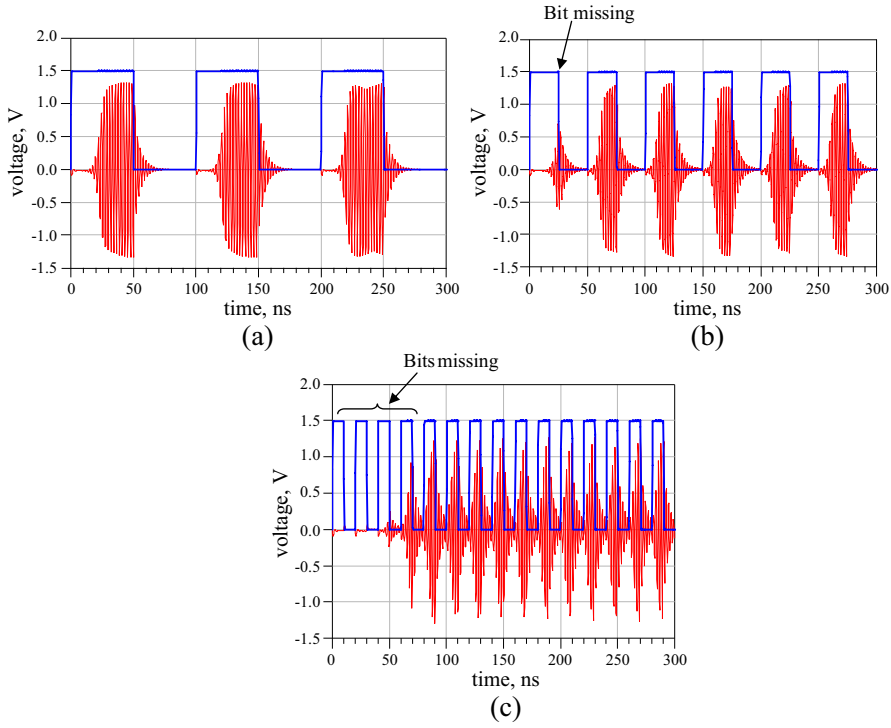

Figure 6. OOK-modulated signal at three data transmission rates: (a) 20 Mb/s, (b) 40 Mb/s, (c) 100 Mb/s.

up time significantly, but it increases power consumption and the complexity of the circuit. Rather than using tail current biasing circuit, we used two other techniques to reduce the delay in the start-up of the oscillator, i.e., MOS transistor's capacitance matching and tank optimization. MOS transistor's capacitance matching requires redesigning the active network with Equation (5) to make the gate sizes equal. Since L_{M_1} and L_{M_2} are fixed at 0.18 µm, we set W_{M_1} and W_{M_2} at 100 µm, which reduced the start-up time from the 40 ns required in the previous design to 20 ns (Figure 7(a)). Although, this redesign of the active network reduced the PN performance to −128 dBc, it was still acceptable for operation. In the optimization of the LC tank, the maximum possible L_1 value also reduced start-up delay, which also increased the peak-to-peak swings in the output voltage of the oscillator. The maximum supported L_1 value, i.e., 34 nH, required reducing the C_1 value from 7 pF to 3 pF, and that reduced the start-up time to 6 ns (Figure 7(b)).

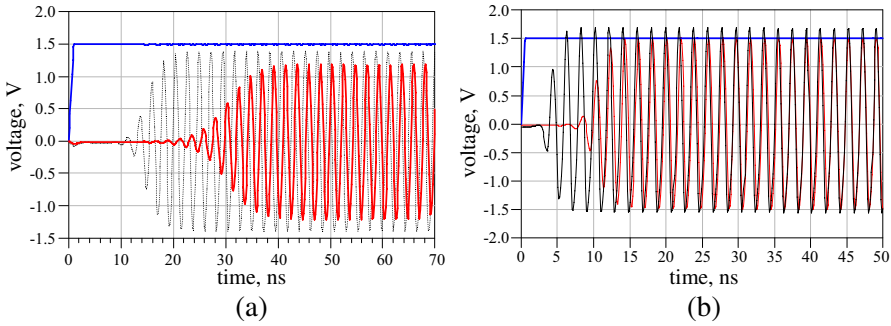

Figure 7. Optimized start-up time for the oscillator: (a) Performance before capacitance matching (solid curve) and after capacitance matching (dashed curve). (b) Performance before tank circuit optimization (solid curve) and after tank circuit optimization (dashed curve).

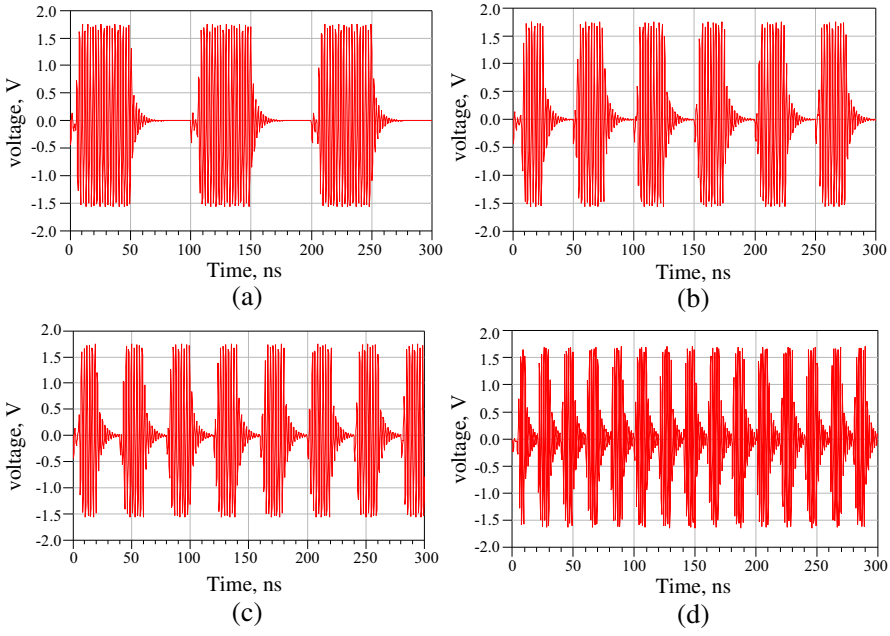

Figure 8. OOK-modulated signal after optimizing start-up time at (a) 20 Mb/s, (b) 40 Mb/s, (c) 50 Mp/s, (d) 100 Mb/s.

Figure 8 shows the output signal of the OOK-modulated oscillator at four different data transmission rates, i.e., 20 Mb/s, 40 Mb/s, 50 Mb/s, and 100 Mb/s. At the data transmission rate of 100 Mbps, the bit duration was 10 ns; therefore, the 6-ns start-up time was rapid enough to run the oscillator by pulse data at 100 Mb/s without any initial bit loss (Figure 8(d)). However, at the higher data transmission rate, the decay period of the oscillator, t_d, was greater than the bit duration (Figure 8(d)), which made it more difficult to reconstruct data at the receiving end. The envelop filter was designed to overcome this problem, with the NMOSs being sized to 3/0.18 µm to minimize the losses of the envelop-filter circuit. The OOK signal after the envelop filter is shown in Figure 9. The envelop filter attenuated the OOK modulated signal by 3 dBm. The spectra of the modulated signal at different data transmission rates are shown in Figure 10. Although the spectrum power was reduced slightly at the higher data transmission rate, the spectrum power was approximately 5 dBm. When the carrier signal was turned on and off by the modulating signal in the OOK system, an additional frequency component is added to

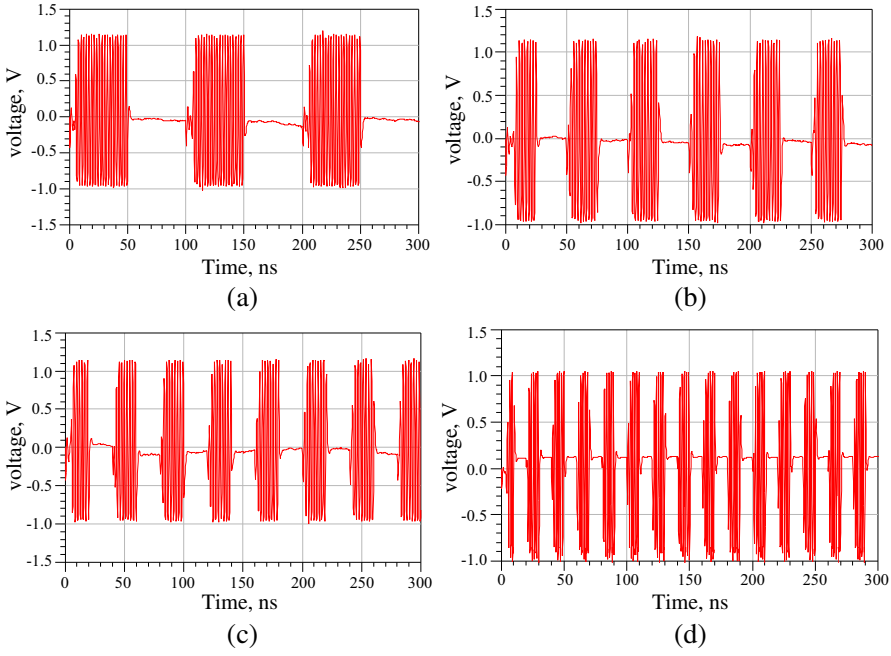

Figure 9. OOK-modulated signal after the envelop filter at (a) 20 Mb/s, (b) 40 Mb/s, (c) 50 Mp/s, (d) 100 Mb/s.

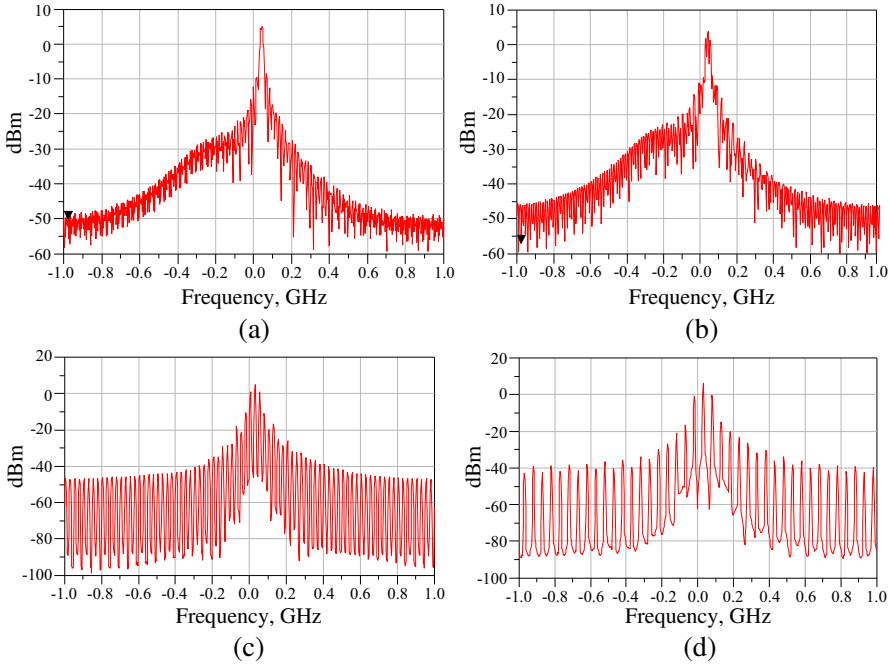

Figure 10. Signal spectra of envelope filtered signal at (a) 20 Mb/s, (b) 40 Mb/s, (c) 50 Mp/s, (d) 100 Mb/s.

the carrier frequency, which increased the bandwidth of the system. This additional frequency component depended on the rate at which the carrier signal was turned on and off. Therefore, the higher the rate of on and off was, the higher the bandwidth of the transmitting signal became.

However, the 1.5 V, V-high of pulse data was important because the overall performance of the transmitter was changed with the lower the V-high than the 1.5 V. The start-up time and peak-to-peak swings in the output voltage of the oscillator decreased as the voltage level of the data bit decreased which made the system unstable high data transmission rates and the oscillating frequency shifted to the upper scale as the voltage decreased. Table 2 shows the effect of voltage drop on the data bits. From Equation (6), a single-stage, L-section, impedance-matching circuit was used to match the $726 + j5\,\Omega$-output impedance to the 50-Ω load. The simulated reflection coefficient of the matching network with 45 nH, L_2, and 2.5 pF C_2 is shown in Figure 11. At the centre frequency, the reflection coefficient was less than -35 dB.

Table 2. Performance shifting of transmitter with different V-high values.

V-high	Start-up Time (t_{s-u})	Spectrum Power	Frequency shift
1.1	30 ns	−8.35 dBm	450 + 24 MHz
1.2	15 ns	6 dBm	450 + 19 MHz
1.3	10 ns	8 dBm	450 + 13 MHz
1.4	8 ns	9 dBm	450 + 7 MHz
1.5	6 ns	10 dBm	450 + 0 MHz

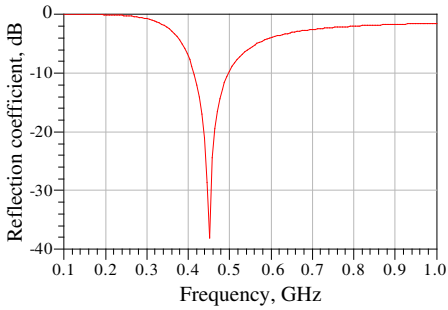

Figure 11. Reflection coefficient of matching network.

5. CONCLUSIONS

In this paper, we presented a novel, high-speed, 450-MHz, transmitter system for WCE applications. The proposed transmitter eliminates the complicated building block and the external components that use excessive power. The transmitter system was optimized with various low-power techniques and by considering the path losses that occur in the human body. Our optimized transmitter can operate with only 25% of the power required by a conventional transmitter, so it can be operated by 1.5 V pulse data. The oscillator has a rapid start-up time of only 6 ns, which is sufficient for operating the transmitter at a data transmission rate of 100 Mbps. The maximum swing in the peak-to-peak voltage of the oscillator resulted in an output power of almost 5 dBm. The entire system was simulated in a 0.18-µm CMOS process. The proposed transmitter is highly suited for the high-resolution images and high transmission rates required for successful use in WCE applications.

ACKNOWLEDGMENT

The authors are grateful to the Ministry of Higher Education, Malaysia, for the financial support provided for this research work under grant FRGS/FASA/TAHUN/SKK/JPP/03/6 via Politeknik Tuanku Syed Sirajuddin.

REFERENCES

1. Iddan, G., G. Meron, A. Glukhovsky, and P. Swain, "Wireless capsule endoscopy," *Nature*, Vol. 405, 417, May 2000.
2. Pan, G. and L. Wang, "Swallowable wireless capsule endoscopy: Progress and technical challenges," *Gastroenterology Research and Practice*, Vol. 2012, 1–9, 2011.
3. Ciuti, G., A. Menciassi, and P. Dario, "Capsule endoscopy: From current achievements to open challenges," *IEEE Reviews in Biomedical Engineering*, Vol. 4, 59–72, 2011.
4. Chi, B., J. Yao, S. Han, X. Xie, G. Li, and Z. Wang, "Low power high data rate wireless endoscopy transceiver," *Microelectronics Journal*, Vol. 38, 1070–1081, 2007.
5. Chi, B., J. Yao, S. Han, X. Xie, G. Li, and Z. Wang, "Low-power transceiver analog front-end circuits for bidirectional high data rate wireless telemetry in medical endoscopy applications," *IEEE Transactions on Biomedical Engineering*, Vol. 54, 1291–1299, 2007.
6. Diao, S., Y. Zheng, and C. Heng, "A CMOS ultra low-power and highly efficient UWB-IR transmitter for WPAN applications," *IEEE Transactions on Circuits and Systems II: Express Briefs*, Vol. 56, 200–204, 2009.
7. Gao, Y., Y. Zheng, S. Diao, W. Toh, C. Ang, M. Je, and C. Heng, "Low-power ultrawideband wireless telemetry transceiver for medical sensor applications," *IEEE Transactions on Biomedical Engineering*, Vol. 58, 768–772, 2011.
8. Shaban, H. A. and M. A. El-Nasr, "Performance comparison of ED, TR and DTR IR-UWB receivers for combined PAM-PPM modulation in realistic UWB channels," *Progress In Electromagnetics Research Letters*, Vol. 30, 91–103, 2012.
9. Wong, S.-K., F. Kung, S. Maisurah, and M. N. B. Osman, "A WiMedia compliant CMOS RF power amplifier for ultra-wideband (UWB) transmitter," *Progress In Electromagnetics Research*, Vol. 112, 329–347, 2011.
10. Basar, M. R., M. F. B. A. Malek, K. M. Juni, M. I. M. Saleh,

M. S. Idris, L. Mohamed, N. Saudin, N. A. Mohd Affendi, and A. Ali, "The use of a human body model to determine the variation of path losses in the human body channel in wireless capsule endoscopy," *Progress In Electromagnetics Research*, Vol. 133, 495–513, 2013.

11. Theilmann, P., M. A. Tassoudji, E. H. Teague, D. F. Kimball, and P. M. Asbeck, "Computationally efficient model for UWB signal attenuation due to propagation in tissue for biomedical implants," *Progress In Electromagnetics Research B*, Vol. 38, 1–22, 2012.
12. Szczepkowski, G., J. Dooley, and R. Farrell, "The concept of CMOS OOK transmitter using low voltage self-oscillating active inductor," *International Conference on Signals and Electronics Systems,* 213–216, 2010.
13. Diao, S., Y. Zheng, Y. Gao, C. Heng, and M. Je, "A 7.2-mW, 15-Mbps ASK CMOS transmitter for ingestible capsule endoscopy," *IEEE Asia Pacific Conference on Circuits and Systems (APCCAS)*, 512–515, Dec. 6–9, 2010.
14. Kim, K., S. Yun, S. Lee, S. Nam, Y. Yoon, and C. Cheon, "A design of a high-speed and high-efficiency capsule endoscopy system," *IEEE Transactions on Biomedical Engineering*, Vol. 59, 1005–1011, Apr. 2012.
15. Anang, K. A., P. B. Rapajic, R. Wu, L. Bello, and T. I. Eneh, "Cellular system information capacity change at higher frequencies due to propagation loss and system parameters," *Progress In Electromagnetics Research B*, Vol. 44, 191–221, 2012.
16. Anang, K. A., P. B. Rapajic, L. Bello, and R. Wu, "Sensitivity of cellular wireless network performance to system & propagation parameters at carrier frequencies greater than 2 GHz," *Progress In Electromagnetics Research B*, Vol. 40, 31–54, 2012.
17. Van Laethem, B., F. Quitin, F. Bellens, C. Oestges, and P. De Doncker, "Correlation for multi-frequency propagation in urban environments," *Progress In Electromagnetics Research Letters*, Vol. 29, 151–156, 2012.
18. Ibrani, M., L. Ahma, E. Hamiti, and J. Haxhibeqiri, "Derivation of electromagnetic properties of child biological tissues at radio frequencies," *Progress In Electromagnetics Research Letters*, Vol. 25, 87–100, 2011.
19. Chen, Z. and Y.-P. Zhang, "Effects of antennas and propagation channels on synchronization performance of a pulse-based ultra-wideband radio system," *Progress In Electromagnetics Research*, Vol. 115, 95–112, 2011.
20. Theilmann, P., M. A. Tassoudji, E. H. Teague, D. F. Kimball, and

P. M. Asbeck, "Computationally efficient model for UWB signal attenuation due to propagation in tissue for biomedical implants," *Progress In Electromagnetics Research B*, Vol. 38, 1–22, 2012.

21. Izdebski, P. M., H. Rajagopalan, and Y. Rahmat-Samii, "Conformal ingestible capsule antenna: A novel chandelier meandered design," *IEEE Transactions on Antennas and Propagation*, Vol. 57, No. 4, 900–909, Apr. 2009.
22. Kwak, K. S., S. Ullah, and N. Ullah, "An overview of IEEE 802.15.6 standard," *3rd International Symposium on Applied Sciences in Biomedical and Communication Technologies (ISABEL)*, 1–6, Nov. 7–10, 2010.
23. Chirwa, L., C. P. A. Hammond, S. Roy, and D. R. S. Cumming, "Electromagnetic radiation from ingested sources in the human intestine between 150 MHz and 1.2 GHz," *IEEE Transactions on Biomedical Engineering*, Vol. 50, No. 4, 484–492, Apr. 2003.
24. Vidal, N., S. Curto, J. M. Lopez-Villegas, J. Sieiro, and F. M. Ramos, "Detuning study of implantable antennas inside the human body," *Progress In Electromagnetics Research*, Vol. 124, 265–283, 2012.
25. Zhang, M. and A. Alden, "Calculation of whole-body SAR from a 100 MHz dipole antenna," *Progress In Electromagnetics Research*, Vol. 119, 133–153, 2011.
26. Vrbova, B. and J. Vrba, "Microwave thermotherapy in cancer treatment: Evaluation of homogeneity of SAR distribution," *Progress In Electromagnetics Research*, Vol. 129, 181–195, 2012.
27. Moglie, F., V. Mariani Primiani, and A. P. Pastore, "Modeling of the human exposure inside a random plane wave field," *Progress In Electromagnetics Research B*, Vol. 29, 251–267, 2011.
28. Aguirre, E., J. Arpon, L. Azpilicueta, S. De Miguel Bilbao, V. Ramos, and F. J. Falcone, "Evaluation of electromagnetic dosimetry of wireless systems in complex indoor scenarios with human body interaction," *Progress In Electromagnetics Research B*, Vol. 43, 189–209, 2012.
29. Ronald, S. H., M. F. B. A. Malek, S. H. Idris, E. M. Cheng, M. H. Mat, M. S. Zulkefli, and S. F. Binti Maharimi, "Designing asian-sized hand model for SAR determination at GSM900/1800: Simulation part," *Progress In Electromagnetics Research*, Vol. 129, 439–467, 2012.
30. Kwon, Y., S. Park, T. Park, K. Cho, and H. Lee, "An ultra low-power CMOS transceiver using various low-power techniques for LR-WPAN applications," *IEEE Transactions on Circuits and Systems I: Regular Papers*, Vol. 59, 324–336, Feb. 2012.

31. Basar, M. R., F. Malek, K. M. Juni, M. I. M. Saleh, and M. Shaharom Idris, "A low power 2.4-GHz current reuse VCO for low power miniaturized transceiver system," *IEEE International Conference on Electronic Design, Systems and Applications*, 215–218, 2012.
32. Rogers, J. W. M. and C. Plett, *Radio Frequency Integrated Circuit Design*, 2nd Edition, Artech House, Boston, London, 2010.
33. Fong, N., C. Plett, G. Tarr, J.-O. Plouchart, D. Liu, N. Zamdmer, and L. Wagner, "Phase noise improvement of deep submicron low voltage VCO," *Proceedings of the 28th European Solid-State Circuits Conference*, 811–814, Sep. 24–26, 2002.
34. Kim, J. H. and M. M. Green, "Fast startup of LC VCOs using circuit asymmetries," *20th European Conference on Circuit Theory and Design,* 2011.
35. Diao, S., Y. Zheng, and C. Heng, "A CMOS ultra low-power and highly efficient UWB-IR transmitter for WPAN application," *IEEE Trans. on Circuits and Systems — II,* Vol. 56, 200–204, Mar. 2009.
36. Barras, D., F. Ellinger, H. Jackel, and W. Hirt, "Low-power ultra-wideband wavelets generator with fast start-up circuit," *IEEE Trans. on Microwave Theory and Technique*, Vol. 54, 2138–2145, May 2006.
37. Barras, D., F. Ellinger, H. Jackel, and W. Hirt, "Low-power ultra-wideband wavelets generator with fast start-up circuit," *IEEE Transactions on Microwave Theory and Techniques*, Vol. 54, 2138–2145, May 2006.
38. Diao, S., Y. Zheng, and C.-H. Heng, "A CMOS ultra low-power and highly efficient UWB-IR transmitter for WPAN applications," *IEEE Transactions on Circuits and Systems II: Express Briefs*, Vol. 56, 200–204, Mar. 2009.
39. Everitt, W. L., and G. E. Anner, *Communication Engineering*, 3rd Edition, McGraw-Hill, New York, 1956.
40. Han, Y. and D. J. Perreault, "Analysis and design of high efficiency matching networks," *IEEE Transactions on Power Electronics,* Vol. 21, 1484–1491, Sep. 2006.
41. Misra, D. K., *Radio-frequency and Microwave Communication Circuits*, John Wiley & Sons, Inc., 2004.